JACS
JOURNAL OF THE AMERICAN CHEMICAL SOCIETY
Article
pubs.acs.org/JACS

Intestinal Permeability of Cyclic Peptides: Common Key Backbone Motifs Identified

Johannes G. Beck,[†] Jayanta Chatterjee,[†] Burkhardt Laufer,[†] Marelli Udaya Kiran,[†] Andreas O. Frank,[†] Stefanie Neubauer,[†] Oded Ovadia,[§] Sarit Greenberg,[§] Chaim Gilon,[‡] Amnon Hoffman,[§] and Horst Kessler*[,†,∥]

[†]Institute for Advanced Study and Center for Integrated Protein Science at the Technische Universität München, Department Chemie, Lichtenbergstrasse 4, 85747 Garching, Germany

[‡]Institute of Chemistry, The Hebrew University of Jerusalem, Jerusalem 91904, Israel

[§]Institute of Drug Research, The Hebrew University of Jerusalem, Jerusalem 91120, Israel

[∥]Chemistry Department, King Abdulaziz University, Saudi Arabia

Supporting Information

ABSTRACT: Insufficient oral bioavailability is considered as a key limitation for the widespread development of peptides as therapeutics. While the oral bioavailability of small organic compounds is often estimated from simple rules, similar rules do not apply to peptides, and even the high oral bioavailability that is described for a small number of peptides is not well understood. Here we present two highly Caco-2 permeable template structures based on a library of 54 cyclo(-D-Ala-Ala$_5$-) peptides with different *N*-methylation patterns. The first (all-*trans*) template structure possesses two β-turns of type II along Ala^6-D-Ala^1 and Ala^3-Ala^4 and is only found for one peptide with two *N*-methyl groups at D-Ala^1 and Ala^6 [(**NMe(1,6)**]. The second (single-*cis*) template possesses a characteristic *cis* peptide bond preceding Ala^5, which results in type VI β-turn geometry along Ala^4-Ala^5. Although the second template structure is found in seven peptides carrying *N*-methyl groups on Ala^5, high Caco-2 permeability is only found for a subgroup of two of them [**NMe(1,5)** and **NMe(1,2,4,5)**], suggesting that *N*-methylation of D-Ala^1 is a prerequisite for high permeability of the second template structure. The structural similarity of the second template structure with the orally bioavailable somatostatin analog cyclo(-Pro-Phe-*N*Me-D-Trp-*N*Me-Lys-Thr-*N*Me-Phe-), and the striking resemblance with both β-turns of the orally bioavailable peptide cyclosporine A, suggests that the introduction of bioactive sequences on the highly Caco-2 permeable templates may result in potent orally bioavailable drug candidates.

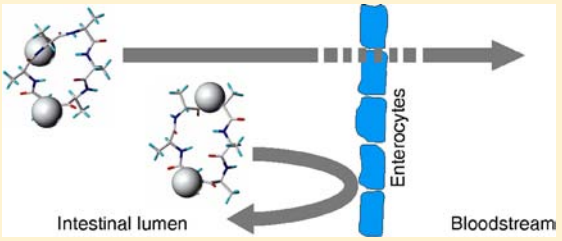

INTRODUCTION

Oral bioavailability is still one of the most appreciated properties of drugs. Empirical rules such as Lipinski's "rule of 5" or Veber's rules consider physicochemical parameters such as the number of rotatable bonds and hydrophobic patch size in order to filter out drug candidates that are suggested not to be absorbed into the bloodstream upon oral administration.[1,2] However, as described by Zhang and Wilkinson in 2007,[3] 20% of all FDA-approved oral drugs did not agree with the "rule of 5" criteria and only 70% of the drugs that fulfilled these criteria had been approved for oral use (based on FDA-approved drugs in 2007). Accordingly, compliance with simple criteria such as the "rule of 5" neither guarantees oral bioavailability, nor does the violation of such criteria reliably predict insufficient oral bioavailability.

However, as suggested by the "rule of 5", most peptides are not (or almost not) orally bioavailable. On the other hand, a number of peptides are surprisingly well absorbed within the gastrointestinal (GI) tract. Amanitins,[4] phalloidin,[2] antamanide,[2] cyclosporine A,[5,6] some cyclic hexa- and octapeptidic somatostatin analogs,[7−9] microcystin LR,[10] and a cyclic agonist of melanocortin receptor subtype 4[11] possess significant oral bioavailability and/or intestinal permeability. Despite an oral bioavailability of only 0.1%,[12] the vasopressin analog desmopressin[13] is (also) used orally. Moreover, several *N*-alkylated natural cyclopeptides and depsipeptides, e.g. from marine origin such as hepatotoxic nodularins,[14] can lead to intoxication in animals.[15−17] Unfortunately, scientific publications describing explicitly the oral bioavailability of such compounds are very rare.

In a recent comprehensive study, the Lokey group[18] identified membrane permeating orally bioavailable peptide scaffolds. One of the most permeable compounds (cyclo[Leu-*N*Me-D-Leu-*N*Me-Leu-Leu-D-Pro-*N*Me-Tyr]) possessed an impressive oral bioavailability of 28% in rat.[18] In earlier studies headed by Lokey, cyclopeptide conformations were predicted successfully[19] and the membrane permeability of non-*N*-methylated stereoisomers of cyclo[Leu-Leu-Leu-Leu-Pro-Tyr] was traced back to intramolecular hydrogen bond networks, to

Received: April 3, 2012
Published: June 27, 2012

   dx.doi.org/10.1021/ja303200d | J. Am. Chem. Soc. 2012, 134, 12125−12133

steric protection of amide hydrogen atoms from the solvent, and to the relative stability of impermeable conformers in water.[20]

In an attempt to understand the intestinal permeability of various differentially charged linear and constrained cyclic peptides, the Borchardt group pointed out the importance of the conformational flexibility and threshold molecular radii of the peptides permeating the intestinal mucosa.[21] Moreover, they suggest interplay of various physicochemical properties instead of just one in modulating the permeation of hydrophilic peptides.[22] In a study of model peptides comprising N-methylated peptides, they also pointed out the importance of the hydrogen bonding potential in contrast to the lipophilicity of the studied peptides.[23] Furthermore, they also suggested that the compactness of the cyclic peptides by maximizing the intramolecular hydrogen bonding in aqueous solution mainly influences their permeability.[24]

In spite of the observation that oral bioavailability is preferably found for cyclic and *N*-methylated peptide analogs, the structural features that are responsible for the oral bioavailability of peptides are not well understood. The rational design of peptide drugs that possess sufficient oral bioavailability is therefore still a daunting task. A clearer understanding of the structural properties that make some peptides cross the gastrointestinal tract into the bloodstream would promote the development of peptides as drugs. As in peptides, Φ, Ψ, and χ dihedrals can adopt many different angles; structural properties favoring oral bioavailability can only be identified in three-dimensional structures.

The different mechanisms that seem to operate in the absorption of the structurally heterogeneous orally bioavailable peptides introduce a further level of complexity to delineate the absorption of orally available peptides in the GI tract in terms of structural properties. The most important mechanisms for the absorption of drugs in the intestine include passive diffusion through enterocytes (transcellular pathway), passive paracellular diffusion (paracellular pathway), endo-/exocytosis, active transport via various peptide transporters (e.g., the dipeptide carrier), and the release from enterocytes back into the lumen by p-glycoprotein.[25] While internal hydrogen bond formation and masking of external hydrogen bond donors clearly suggests membrane permeation (transcellular pathway) for most of the lipophilic peptides, e.g. *N*-methylated cyclo(-Leu-Leu-Leu-Leu-Pro-Tyr-),[18] there seems to be another route involved for the transport of peptides that possess multiple polar side-chains, such as α-amanitin[4] or phalloidin, which is transported via interaction with bile salt binding polypeptides.[26,27]

The extensive study toward understanding the intestinal permeability of a library of 54 differently *N*-methylated cyclo(-D-Ala-Ala$_5$-) peptides showed that multiple *N*-methylation could dramatically improve their Caco-2 permeability. Although the exact transport route of these peptides was not fully characterized, the data, however, suggested a facilitated diffusion.[28]

The permeation of Caco-2 monolayers indicated a variable pattern for potential oral bioavailability of cyclo(-D-Ala-Ala$_5$-) peptides, depending upon the site and number of *N*-methylations. The highest Caco-2 permeation was observed for eight peptides that possessed either two or four *N*-methyl groups (Figure 1B–D). The Caco-2 permeation of these peptides was similar to that of testosterone ($P_{app} > 1 \times 10^{-5}$ cm/s) or even higher (testosterone: marker of transcellular permeability). On the other hand, the vast majority of the other 46 peptides possessed much lower Caco-2 permeability, similar to or even less than that of mannitol ($P_{app} < 1 \times 10^{-6}$ cm/s), a marker for paracellular permeability.

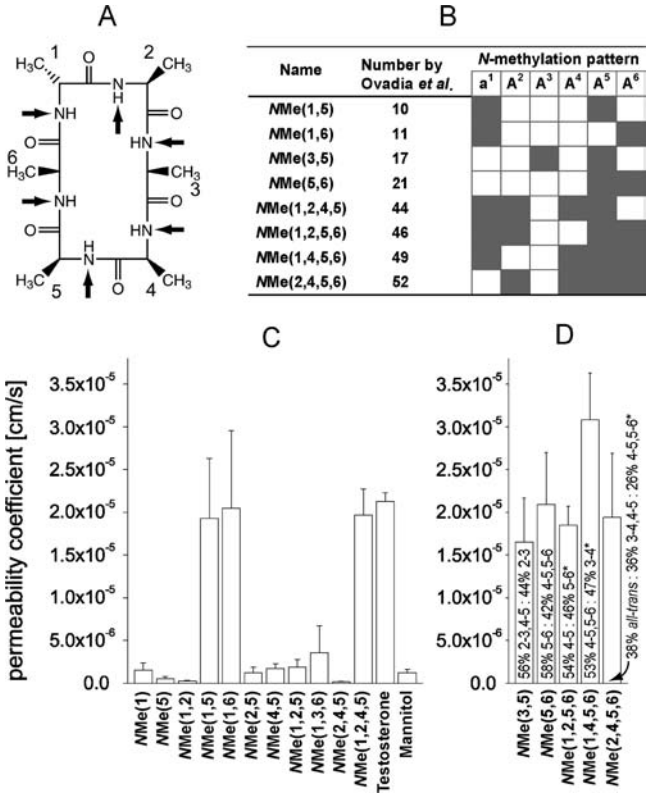

Figure 1. (A) *N*-Methylated cyclo(-D-Ala-Ala$_5$-) peptides described by Ovadia et al.[28] (B) *N*-Methylation pattern of eight peptides that possess the highest Caco-2 permeability. (C) Caco-2 permeability coefficients of all conformationally homogeneous peptides, and (D) Caco-2 permeability coefficients of heterogeneous peptides that are considered for structural analysis. The numbers in the bars denote the population of the conformers (%) and the sites of *cis* peptide bonds. The permeability coefficients obtained for testosterone and mannitol are shown for comparison in panel C. (*) Additional minor conformations were observed.

RESULTS AND DISCUSSION

Lipophilicity and Permeation Pathway. In the PAMPA$_{lecithin}$ tests, none of the better performing Caco-2 permeable peptides crossed the artificial membrane, suggesting the mechanism of intestinal permeability is not merely transcellular.[28] Moreover, the reversed phase HPLC of these peptides revealed shorter retention times, in contrast to the case of testosterone, which eluted much more slowly. This observation did not correlate with the high Caco-2 permeation rates of the peptides (Figure 2). Similar to PAMPA tests, this suggested a considerably higher lipophilicity of testosterone, as compared to those of all the peptides. Moreover, the HPLC experiment suggests similar hydrophobicities for peptides with very similar chemical structures, which have extremely different Caco-2 permeabilities. In spite of the high Caco-2 permeation rates of these peptides (comparable to the permeability of testosterone), the transcellular diffusion mechanism must therefore be excluded. This clearly suggests that other mechanisms lead to the high Caco-2 permeation rates as opposed to the one suggested by White et al. for the orally

dx.doi.org/10.1021/ja303200d | J. Am. Chem. Soc. 2012, 134, 12125–12133

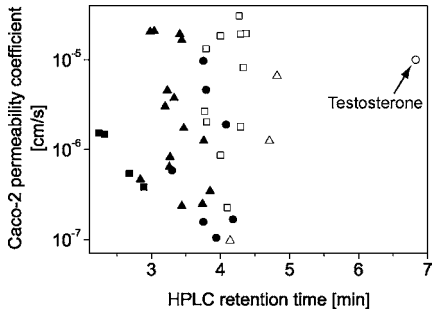

Figure 2. HPLC retention time and Caco-2 permeation of single (■), double (▲), triple (●), tetra (□), and penta (Δ) *N*-methylated cyclo(-D-Ala-Ala_5-) peptides, and testosterone (○).

bioavailable *N*-methylated stereoisomers of cyclo(-Leu-Leu-Leu-Leu-Pro-Tyr-).[18]

Based on the chemical constitution of the highly permeable peptides, almost no common structural properties could be assigned besides the presence of either two or four *N*-methyl groups.[28] Therefore, a detailed conformational analysis was performed to identify the three-dimensional structural elements, which underline high Caco-2 permeability.

NMR Conformational Studies. For 43 out of 54 peptides, two or more sets of ^{1}H NMR signals indicated equilibria of two or more preferred *cis*−*trans* isomers with a minor population of at least 5%. Side-conformers (*cis*−*trans* isomer populations ≥5%) were observed not only for weakly permeable peptides but also for five of the eight highly permeable peptides (Figure 1D). In addition to the highly Caco-2 permeable peptides, three-dimensional structures were also derived for conformationally homogeneous peptides (Figure 1C); as for these peptides, the observed Caco-2 permeability could be analyzed based on a single preferred conformation. Among the eleven conformationally homogeneous peptides (Figure 1C) and the five conformationally heterogeneous peptides under investigation (Figure 1D), only ***N*Me(1,6)**, ***N*Me(1,5)**, and ***N*Me-(1,2,4,5)** were found to possess both high permeability and conformational homogeneity. These peptides were considered as highly Caco-2 permeating structures (Figure 3) and served as templates for the analysis of other conformationally homogeneous or well permeable peptides. For the other highly permeable peptides ***N*Me(3,5)**, ***N*Me(5,6)**, ***N*Me(1,2,5,6)**, and ***N*Me(1,4,5,6)**, two preferred conformations and, for ***N*Me-(2,4,5,6)**, even three preferred conformations had to be considered.

First Template Structure. The first template structure is represented by the conformationally homogeneous peptide ***N*Me(1,6)**. It possesses a typical all-*trans* cyclohexapeptide structure with two opposite type II *β*-turns (Figure 3). *N*Me Ala^6 and *N*Me D-Ala^1 are located in positions *i* + 1 and *i* + 2 of one of these turns. A characteristic hydrogen bond is formed

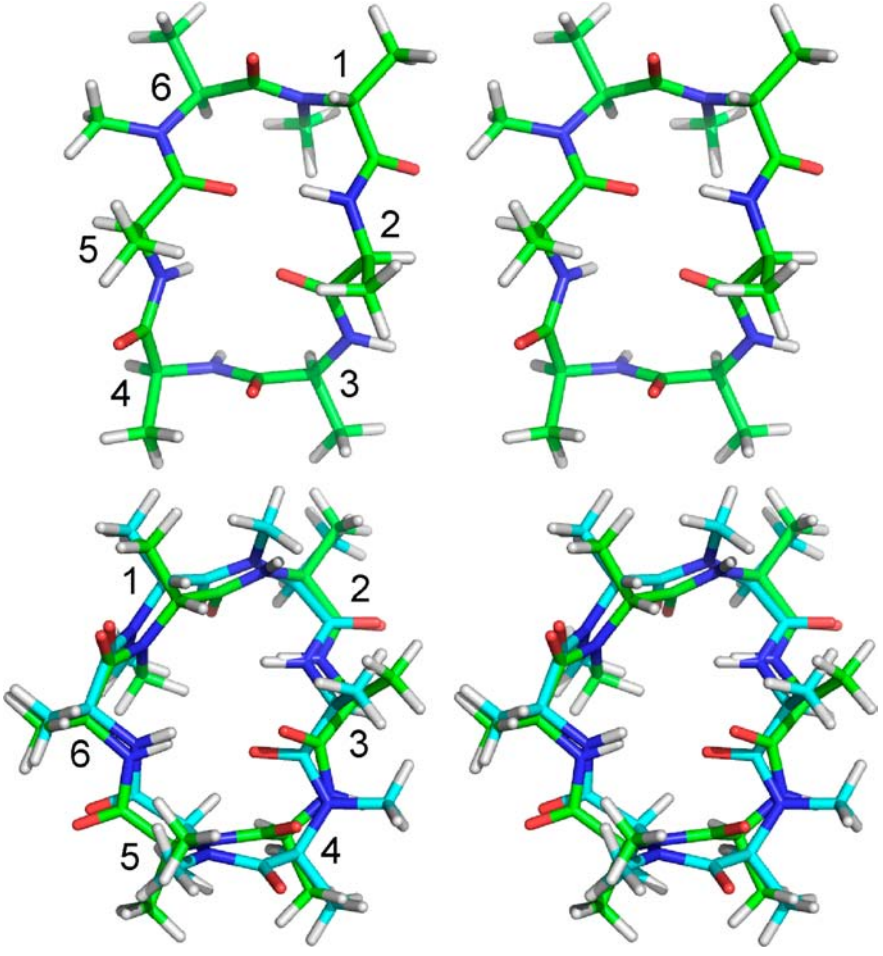

Figure 3. Stereostructures of conformationally homogeneous Caco-2 cell permeating cyclohexapeptides that are considered as structural templates for a potential high oral bioavailability. Top, ***N*Me(1,6)**; bottom, overlay of ***N*Me(1,5)** and ***N*Me(1,2,4,5)**.

dx.doi.org/10.1021/ja303200d | *J. Am. Chem. Soc.* 2012, 134, 12125−12133

between the carbonyl oxygen atom of the i^{th} residue of this turn (Ala^5 O′) and the amide proton of the i + 3 residue (Ala^2 H^N). Ala^3 and Ala^4 are located in positions i + 1 and i + 2 of the opposite turn. According to MD simulations, the turn along Ala^3-Ala^4 is more flexible than the turn along the *N*-methylated residues. This observation is consistent with an earlier study[29] in which an equilibrium of βI and βII geometry was described for a similar turn in cyclic (-D-Xaa-L-Xaa$_5$-) hexapeptides. Despite this, the turn along Ala^3-Ala^4 also seems to possess a characteristic hydrogen bond between the carbonyl oxygen atom of residue i of this turn (Ala^2 O′) and the amide proton of residue i + 3 (Ala^5 H^N). The amide protons of Ala^2 (7.201 ppm, +0.5 ppb/K) and Ala^5 (7.585 ppm, −1.7 ppb/K) are shifted toward higher fields, and Ala^2 H^N is very efficiently shielded from the solvent, which is well consistent with the hydrogen bonds described above. The structure shown in Figure 3 also agrees with 10 intraresidual, 19 sequential interresidual, and 8 nonsequential interresidual ROEs. The Φ dihedral angles of the protonated amino acids also agree well with the according $^3J_{HN\text{-}H\alpha}$ coupling constants of 9.0 Hz (Ala^2), 4.2 Hz (Ala^3), 7.6 Hz (Ala^4), and 7.8 Hz (Ala^5).

Besides ***N*Me(1,6)**, only four of all the peptides under investigation displayed an all-*trans* conformation. These peptides represent the weakly Caco-2 permeable peptides ***N*Me(1)**, ***N*Me(1,2)**, and ***N*Me(1,3,6)** along with one of three conformers of the highly Caco-2 permeable ***N*Me(2,4,5,6)**.

H^N and C$^\beta$ chemical shifts, the temperature dependence of the H^N chemical shifts, and the $^3J_{HN\text{-}H\alpha}$ coupling constants in the four subsequent residues Ala^3-Ala^6 of ***N*Me(1,2)** are very similar to the respective parameters in the four subsequent residues Ala^2-Ala^5 of ***N*Me(1,6)** (Figure 4). This suggests a high conformational similarity between the structures of ***N*Me(1,2)** and ***N*Me(1,6)**, but with altered sequence positions of the Ala residues (Figure 4A and B).

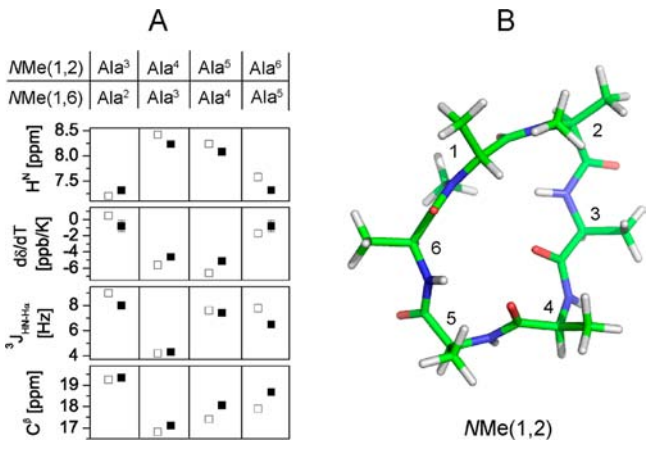

Figure 4. Comparison of H^N chemical shifts, their temperature dependence, $^3J_{HN\text{-}H\alpha}$ couplings, and C$^\beta$ chemical shifts of the four subsequent non-*N*-methylated Ala residues in ***N*Me(1,6)** (□) and ***N*Me(1,2)** (■).

The structure calculated for ***N*Me(1,2)** (Figure 4B) is similar to the one of ***N*Me(1,6)** shown in Figure 3, but there are also significant structural differences to ***N*Me(1,6)** that exceed a simple shift of the peptide sequence along the scaffold. The *N*-methyl group of the peptide bond linking the residues in positions i + 1 and i + 2 of the upper β-turn is pointing up, which indicates a β-turn of type I with *N*Me D-Ala^1 and *N*Me Ala^2 in positions i + 1 and i + 2, respectively. As the peptide bond linking the residues in positions i (Ala^6) and i + 1 (*N*Me Ala^1) is rotated out of the peptide plane, this β-turn does not possess ideal geometry[30] and the characteristic $O'_i - H^N_{i+3}$ hydrogen bond is not formed. The high field shift and low temperature dependence of Ala^3 H^N (7.316 ppm, −0.8 ± 0.7 ppb/K) are indicative for strong shielding from the solvent. Shielding from the solvent is achieved by the internal orientation of the Ala^3 H^N in the peptide ring (see Figure 4B), which is also supported by a strong ROE between Ala^3 H^N and *N*Me Ala^1 H$^\alpha$.

In the lower turn, which is centered at Ala^4 and Ala^5, Ala^5 H^N is pointing down, which indicates similarity to type II β-turn geometry. However, the close proximity of Ala^4 O′ and Ala^6 H^N further indicates the presence of a γ-turn, although it is not absolutely clear whether Ala^6 H^N is hydrogen bonded to Ala^4 O′ or Ala^3 O′. However, strong shielding from the solvent is clearly indicated by a strong shift to higher field (7.320 ppm) and by its low temperature dependence (−0.8 ± 0.7 ppb/K).

As described in more detail in the Supporting Information, for ***N*Me(1)** and ***N*Me(1,3,6)**, multiple fast exchanging conformations have to be assumed.

Second Template Structure. The second Caco-2 permeable template is derived from the conformations of ***N*Me(1,5)** and ***N*Me(1,2,4,5)** (Figure 3). It possesses β-turns about D-Ala^1-Ala^2 and Ala^4-Ala^5. A *cis* peptide bond between Ala^4 and Ala^5 leads to a characteristic type VI geometry for the latter β-turn. A key prerequisite for this conformation is the presence of Ala^5 *N*-methylation, as only this allows for the occurrence of the characteristic *cis* peptide bond. Accordingly, the least *N*-methylated structure that occupies this conformation is ***N*Me(5)** (Figure 5, top). Additional *N*-methylation of D-Ala^1, Ala^2, and Ala^4 does not significantly alter the conformation, as these amide protons are solvent exposed (Figure 5, second row from top). The structure is also conserved in the triply *N*-methylated analogs ***N*Me(1,2,5)** and ***N*Me(2,4,5)** as well as for the tetra *N*-methylated analog ***N*Me(1,2,4,5)**, as shown in Figure 5. As the conformation of this template seems to be highly preferred whenever Ala^3 and Ala^6 are not *N*-methylated, high cooperativity between the upper β-turn with the D-configured residue in position i + 1 and the lower β-turn with type VI geometry has to be assumed.

N*-Methylation at Residue 6 Distorts the Second Template.** As Ala^6 H^N is hydrogen bonded to Ala^3 O′ in the structures with a single *cis* peptide bond between Ala^4 and Ala^5 (Figure 5), *N*-methylation of Ala^6 strongly distorts the overall conformation of the peptide. *N*-Methylation at Ala^6 of the conformationally homogeneous peptides ***N*Me(5)**, ***N*Me-(1,2,5)**, and ***N*Me(2,4,5)**, for example, leads to equilibria of two conformers (N*Me(5,6)**, ***N*Me(1,2,5,6)**) or even three conformers (***N*Me(2,4,5,6)**) (Figure 6). Only in ***N*Me-(1,2,5,6)**, the characteristic conformation with a single *cis* peptide bond between Ala^4 and Ala^5 is conserved but found in equilibrium with a second conformation that possesses a single *cis* peptide bond between Ala^5 and Ala^6. The latter structure is also similar to one ***N*Me(5,6)** conformer, which is found in equilibrium with a second conformer possessing two subsequent *cis* peptide bonds between Ala^4 and Ala^6 (Figure 6). Two ***N*Me(2,4,5,6)** conformers also show two subsequent *cis* peptide bonds between Ala^4 and Ala^6, and between Ala^3 and Ala^5, respectively. In a third conformer, all peptide bonds are in the *trans* configuration, which indicates similarity to the first template structure, rather than similarity to the second template

dx.doi.org/10.1021/ja303200d | J. Am. Chem. Soc. 2012, 134, 12125−12133

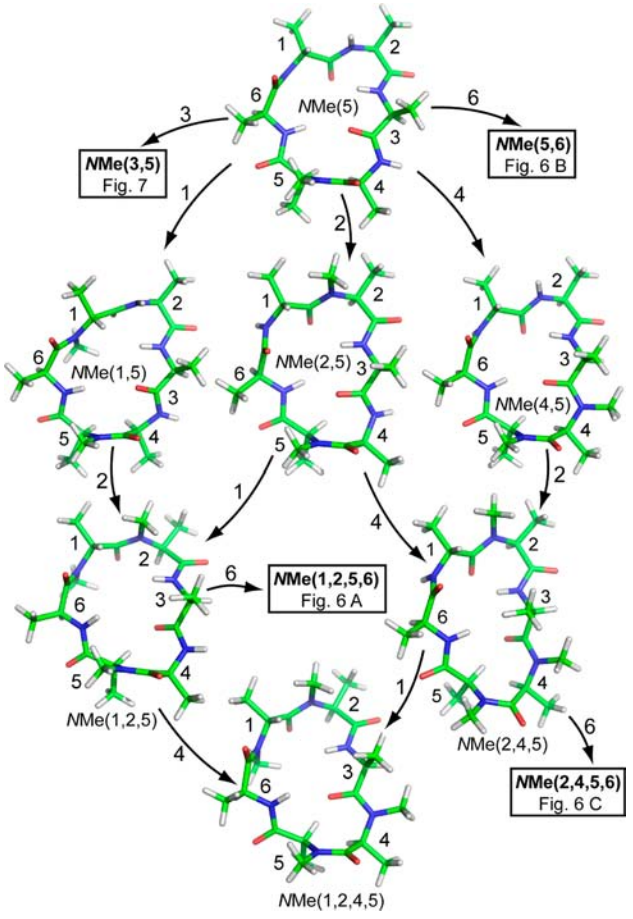

Figure 5. Structures of peptides ***N*Me(5)**, ***N*Me(1,5)**, ***N*Me(2,5)**, ***N*Me(4,5)**, ***N*Me(1,2,5)**, ***N*Me(2,4,5)**, and ***N*Me(1,2,4,5)** are very similar. Starting from ***N*Me(5)** as the parent peptide that possesses the characteristic *cis* peptide bond between residues Ala[4] and Ala[5], the other six peptides can be considered as higher *N*-methylated analogs. The numbers given on the arrows indicate the sequence position on which new *N*-methyl groups are attached. Chemical shifts and their temperature dependence (Supporting Information, Figure S.3) further support the high similarity of the structures shown here.

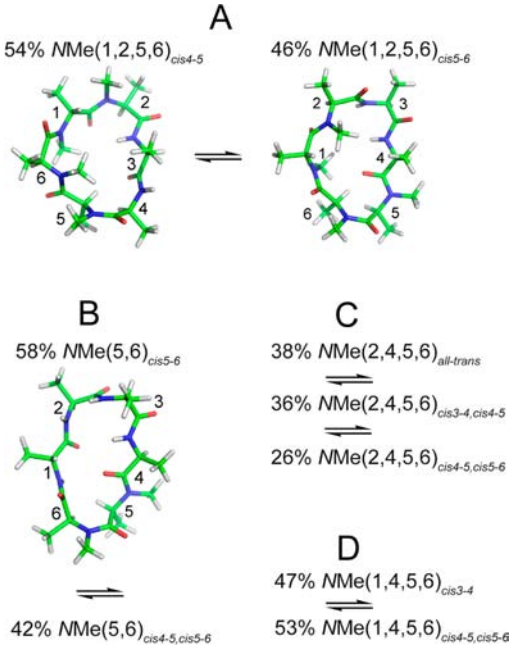

Figure 6. Structures and peptide bond configurations illustrating the effect of *N*-methylation at Ala[6] on peptides possessing the conformation of the second template structure. (A) ***N*Me(1,2,5,6)**, (B) ***N*Me(5,6)**, (C) ***N*Me(2,4,5,6)**, and (D) ***N*Me(1,4,5,6)**. Some conformers could not be derived due to lack of ROEs and the presence of artifacts resulting from exchange effects.

structure. Although the conformation of ***N*Me(1,4,5)** was not investigated due to the presence of a side conformer with a population of 7%, ***N*Me(1,4,5)** most likely represents the same conformation that was found for very similar peptides such as ***N*Me(1,5)** or ***N*Me(1,2,4,5)** (Figure 5). The skewing effect of Ala[6] *N*-methylation is again clearly demonstrated by the *cis*–*trans* pattern of the peptide bonds in ***N*Me(1,4,5,6)**, which originates via the additional *N*-methylation of ***N*Me(1,4,5)** at Ala[6] (Figure 6).

***N*-Methylation at Residue 3 Is Not Tolerated by the Second Template.** Replacement of the H^N atom in the second template (Figure 3, bottom) by a methyl group is not possible due to the spatially restricted orientation of this atom within the cyclopeptide ring. Accordingly, ***N*Me(3,5)** does not occupy the conformation that is characteristic for the second template structure, despite the Ala[5] *N*-methyl group. However, one of the two conformations occupied by ***N*Me(3,5)** possesses a single *cis* peptide bond between Ala[2] and Ala[3] instead, which results in a conformation that is very similar to the second template but with β-turns that are shifted by two sequence positions along the scaffold, such that the upper (lower) turn is centered at Ala[5] and Ala[6] (Ala[2] and Ala[3]). Resemblance of the structures is also confirmed by a high similarity of chemical shifts and temperature gradients of H^N chemical shifts within the Ala[2]-Ala[6] substructure of ***N*Me(1,5)** and the Ala[6]-Ala[4] substructure of ***N*Me(3,5)** (see Table S.17 in the Supporting Information). The ***N*Me(3,5)** conformation with a single *cis* peptide bond between Ala[2] and Ala[3] is thus similar to the ***N*Me(1,5)** but possesses altered configuration of Ala[1] and Ala[3], as indicated in Figure 7.

A similar shift of the peptide sequence along the scaffold with a single *cis* peptide bond was also observed for one of the two conformers found for the peptide with the highest Caco-2 permeability (***N*Me(1,4,5,6)**$_{cis(3-4)}$). In this conformer, the sequence is only shifted by one position along the scaffold, which results in the structure with a *cis* peptide bond between Ala[3] and Ala[4] (positions $i + 1$ and $i + 2$ of the lower β-turn). Accordingly, Ala[6] and D-Ala[1] are found in positions $i + 1$ and $i + 2$ of the upper β-turn (Figure 7). For this conformer, the $^3J_{HN\text{-}H\alpha}$ coupling constants, temperature gradients of H^N chemical shifts, and chemical shifts indicate high structural similarity to ***N*Me(1,2,5,6)**$_{cis(4-5)}$ (Figure 6 A and Table S.18).

For the seven very similar structures shown in Figure 5, variable Caco-2 permeability was observed. Only ***N*Me(1,5)** and ***N*Me(1,2,4,5)** permeate Caco-2 cells efficiently. It is obvious that although *N*-methylation at several positions is tolerated without significant structural alterations, distinct *N*-methylation patterns are required in order to obtain high Caco-2 permeability.

***N*Me[1] Is Needed for Caco-2 Permeability of the Second Template.** The observed low permeability of the four peptides shown in Figure 5 that do not possess Ala[1] *N*-methyl groups on one hand, and the high permeability of ***N*Me(1,5)** and ***N*Me(1,2,4,5)** on the other hand, show that Ala[1] *N*-methylation is essential for the Caco-2 permeability of

dx.doi.org/10.1021/ja303200d | J. Am. Chem. Soc. 2012, 134, 12125–12133

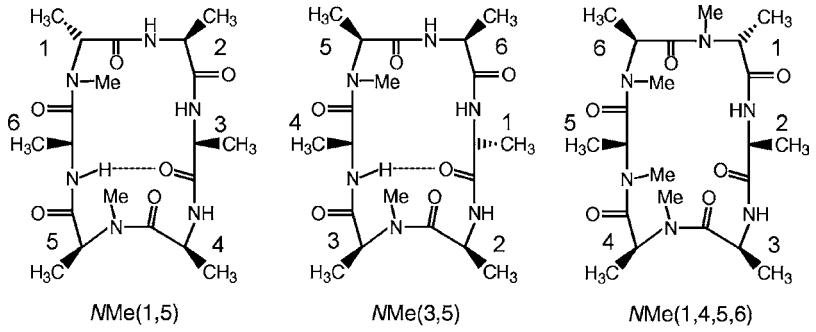

Figure 7. Illustration of the similarity between the structure of ***N*Me(1,5)**, the structure of ***N*Me(3,5)** with a single Ala^2-Ala^3 *cis* peptide bond, and the structure of ***N*Me(1,4,5,6)** with a single Ala^3-Ala^4 *cis* peptide bond. Three-dimensional coordinates were not derived for ***N*Me(3,5)** and ***N*Me(1,4,5,6)** due to artifacts from exchange in the ROESY spectrum and lack of ROEs. Strong ROEs between the H$^\alpha$ nuclei of the residues in positions $i + 1$ and $i + 2$ of the lower turn support our models.

the second template structures. The importance of Ala^1 *N*-methylation for Caco-2 permeation is also supported by the high permeability of ***N*Me(3,5)** and ***N*Me(1,4,5,6)**, which exhibit conformations that possess altered sequence positions on the otherwise identical single *cis* peptide scaffold. As illustrated in Figure 7, the *N*-methylated residues Ala^5 and Ala^6 occupy the $i + 1$ position of the upper β-turn in ***N*Me(3,5)** and ***N*Me(1,4,5,6)**, respectively, a position that is usually occupied by D-Ala^1. It is further important to note that the conformer of ***N*Me(5,6)**, that displays the characteristic single *cis* peptide bond scaffold, does not contain an *N*-methyl group on Ala^2 (which is in the $i + 1$ position of the upper β-turn). However, in contrast to the hydrogen atom in the $i + 1$ position of the upper β-turn, which is solvent exposed in all the structures shown in Figure 5, it points up from the peptide plane and is therefore shielded from the solvent. This may allow for the high permeability of ***N*Me(5,6)** although the *N*-methylation that was described above as crucial for high permeability is not present.

In contrast to the high impact of Ala^1 *N*-methylation on the Caco-2 permeability of the peptides, there is no significant influence of *N*-methylation at Ala^2 and Ala^4, as indicated by the low permeability of the conformationally homogeneous peptides ***N*Me(5)**, ***N*Me(2,5)**, ***N*Me(4,5)**, and ***N*Me(2,4,5)**. The limited contribution of *N*-methylation at Ala^2 and Ala^4 on the Caco-2 permeation is further supported by the similar (high) permeation rates of ***N*Me(1,5)** and ***N*Me(1,2,4,5)**. However, the low permeability of ***N*Me(1,2,5)** in contrast to the high permeability of ***N*Me(1,5)** and ***N*Me(1,2,4,5)** is surprising.

Characteristic Features Modulating the Permeability of the Second Template. Overall, our analysis suggests the following key characteristics for the high Caco-2 permeability of cyclo(-D-Ala-Ala$_5$-) peptides exhibiting the second template structure: (a) one β-turn of type VI with an *N*-methylated *cis* peptide bond between the residues that occupy positions $i + 1$ and $i + 2$; (b) an *N*-methylated residue in position $i + 1$ of the opposing β-turn or shielding of the according amide hydrogen atom from the solvent; (c) the D- and L- configurations of the residues found in positions $i + 1$, $i + 2$, and $i + 3$ of the upper turn apparently do not seem to be important for Caco-2 permeability.

Striking Similarity with Orally Bioavailable Peptides. The three-dimensional structures of some orally bioavailable peptides are similar to the structures of the highly Caco-2 permeable cyclo(-D-Ala-Ala$_5$-) peptides presented above. In the structure of cyclosporin A (CSA) published by Loosli et al.[31] and in the refined structure published by Klages et al.,[32] both β-turns at the ends of the CSA β-strands are similar to the turns in cyclo(-D-Ala-Ala$_5$-) peptides that belong to the second template structure. The upper turn which is centered about D-Ala^1 and Ala^2 in the highly Caco-2 permeating and conformationally homogeneous peptides ***N*Me(1,5)** and ***N*Me(1,2,4,5)** (Figure 3, bottom) is similar to the upper turn of CSA with *N*Me-Gly^3 and *N*Me-Leu^4 in positions $i + 1$ and $i + 2$, respectively (Figure 8A). Please note, that the glycine contains no asymmetric carbon and can therefore easily occupy the position of a D-configured residue. Additionally, the opposite type VI β-turn centered at Ala^4 and Ala^5 in ***N*Me(1,5)** and ***N*Me(1,2,4,5)** is similar to the second turn of CSA with *N*Me-Leu^9 and *N*Me-Leu^{10} in positions $i + 1$ and $i + 2$, respectively (Figure 8B).

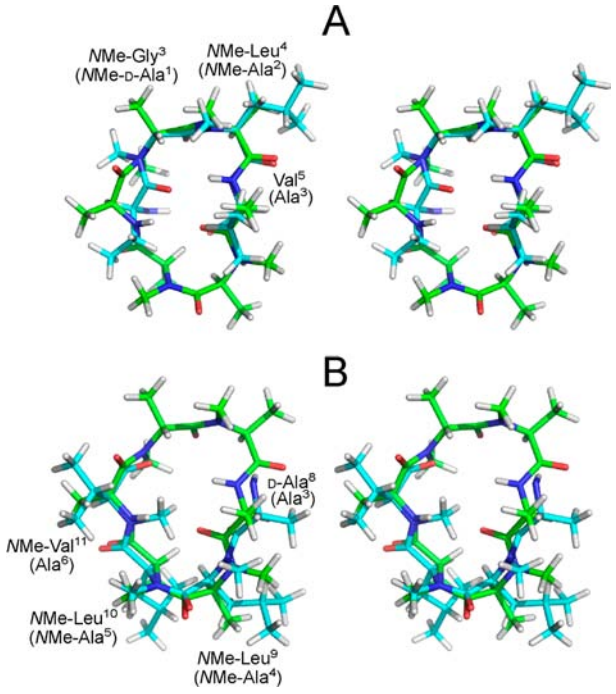

Figure 8. Fit of the type I β-turn of CSA[32] (A) and the type VI β-turn of CSA[32] (B) with the according turns of the highly Caco-2 permeable peptide ***N*Me(1,2,4,5)**. In panels A and B, only the relevant residues of CSA are shown (cyan) together with the according residues of ***N*Me(1,2,4,5)** (green, labels in brackets).

dx.doi.org/10.1021/ja303200d | J. Am. Chem. Soc. 2012, 134, 12125−12133

The similarity of ***N*Me(1,2,4,5)** with the orally bioavailable somatostatin analog cyclo(-Pro-Phe-*N*Me-D-Trp-*N*Me-Lys-Thr-*N*Me-Phe-)[9] is even more striking, as its *N*-methylation pattern is identical to the pattern in ***N*Me(1,2,4,5)**, considering the proline (tertiary amide bond) of the somatostatin analog as an *N*-methylated residue.[33] Additionally, a D-amino acid residue is also present in position $i + 1$ of the upper turn in ***N*Me(1,2,4,5)** and in cyclo(-Pro-Phe-*N*Me-D-Trp-*N*Me-Lys-Thr-*N*Me-Phe-) (Figure 9A).

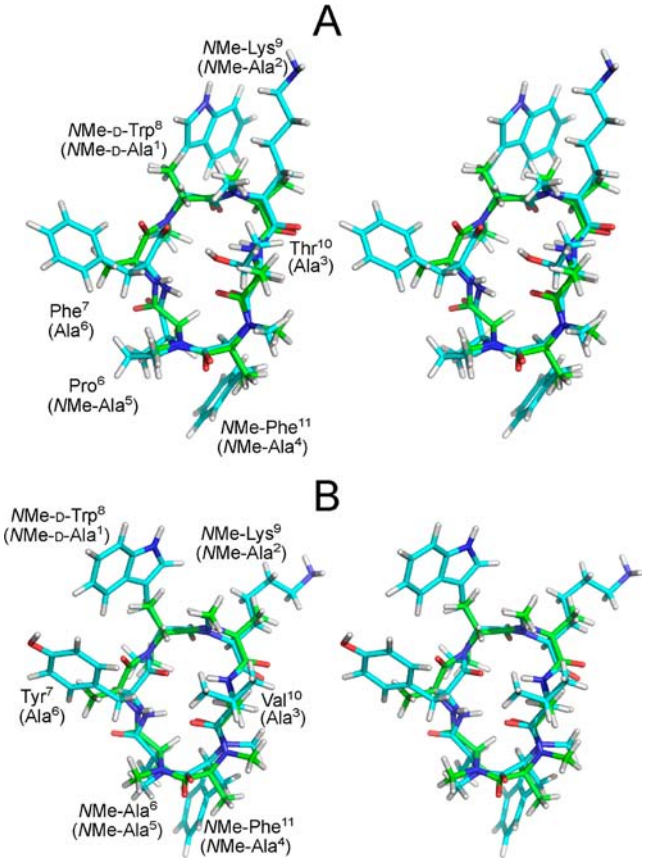

Figure 9. Fit of the cyclo(-Pro-Phe-*N*Me-D-Trp-*N*Me-Lys-Thr-*N*Me-Phe-) (A) and 3-*N*Me-(D-Trp^8,Lys^9,Phe^{11})-seglitide on the *N*Me-(1,2,4,5) solution structures (rmsd(C^α): 0.58 Å (A), 0.64 Å (B)). Somatostatin analogs and *N*Me(1,2,4,5) are shown in white and green color, respectively. Bracketed labels refer to *N*Me(1,2,4,5).

3-*N*Me-(D-Trp^8,Lys^9,Phe^{11})-seglitide (Figure 9 B), another somatostatin analog, possesses a surprisingly high activity in vivo after intraperitoneal injection, as compared to the other seglitide analogs with less *N*-methyl groups but higher sst receptor affinity.[34] Among all the *N*-methylated analogs that were tested, only this analog depicted the *N*-methylation pattern and conformation of the highly Caco-2 permeable cyclic peptide ***N*Me(1,2,4,5)** (Figure 9B). The high in vivo activity of this peptide might be attributed to its improved "drug-like" distribution in rats, as compared to the case of the less *N*-methylated analogs that were investigated in the same study.[34]

When investigating the structure–intestinal permeability relationship of peptides, it should be taken into consideration that the degree of the P_{app} is the sum of the simultaneous permeation kinetics of the tested molecule via the different pathways, as well as the negative contribution of the efflux route. It should also be noted that each permeation pathway requires different structural properties. While the paracellular pathway is via the extracellular matrix that is akin to water-filled channels and thereby requires a polar surface for the molecule, the passive transmembranal permeation necessitates the outer surface to be more lipophilic due to the chemistry of the bilayer membrane. Both these mechanisms are not conformation-selective but are dependent on the nature of the surface. A unique case, which is very likely to be dominant in these tested peptides, is the transporter-mediated internalization. It dictates a very specific conformation similar to the case of receptor–ligand binding. The variability in membrane permeability found among the distinctly *N*-methylated hexapeptides denotes the impact of differences in the 3D-conformation. The highly permeable derivatives have P_{app} values that indicate a transportation higher than that of testosterone, the marker for passive transcellular permeability. Cyclosporin A, which is a highly hydrophobic cyclic *N*-methylated peptide, possesses a conformation comparable to that of the highly permeable hexa-alanine derivative. However, its transport is transcellular with a reduced P_{app} value, due to its known efflux transport by P-glycoprotein (Pgp), also a transporter-mediated phenomenon.[35]

Therefore, one of the major findings in our research is the proof that the mechanism controlling *N*-methylated hexa-alanine permeability is not governed by passive transcellular transport. This is evident by the lack of correlation with the surface polarity indicated by the HPLC retention time, as well as the lack of permeability across the phospholipid monolayer ($PAMPA_{lecithin}$) and, as mentioned before, lack of interaction with the phospholipid surface of colored liposomes.[28] The highly variable permeability properties among the homologous derivatives rule out the possibility of a dominant endocytosis mechanism, as this mechanism is not selective enough to explain the results.

In an overview of the mechanistic permeability of the 54 derivatives with unique positions of the *N*-methyl groups, it is evident to us that the prevailing mechanism of absorption is transporter-mediated permeation. This hypothesis takes into consideration both the high as well as the poor permeabilities, and it highlights the importance of the 3D-conformation imposed by the *N*-methyl groups positioned on the cyclic hexapeptide frame.

It remains to be proven if these observations also hold for peptides with functionalized side chains and if they are mainly controlled by the conformation of the backbone. The case of the somatostatin derivatives (see Figure 9) exhibits that replacement of at least some functional elements is tolerated.

■ CONCLUSION

In conclusion, the extensive conformational studies of the cyclo(-D-Ala-Ala$_5$-) peptides shed light on the structural requirements that convey permeability to these peptides. We show here that solvent shielding of the amide bonds is not the sole factor to impart permeability to the cyclic peptides. We also observe that conformational homogeneity on the time scale of peptide *cis–trans* isomerization does not always guarantee permeability to these peptides and that conformational heterogeneity does not necessarily suppress permeability. On the contrary, the overall structural pattern of the peptides presented here as the template structures governs the permeability property. Employing the cyclo(-D-Ala-Ala$_5$-) peptides, we evaluated the contribution of the backbone

conformation toward permeability of these peptides, and we minimized any side chain contribution. Given the significance of the backbone conformation of the peptide as a crucial factor regulating Caco-2 permeation, alanine residues of permeable cyclo(-D-Ala-Ala$_5$-) peptides may be substituted by pharmacophores to obtain enhanced intestinal permeability of bioactive peptides. A first indication that it is possible to transform the Ala-peptides into biologically functional derivatives with good permeability is presented by cyclosporin A and the *N*-methylated somatostatin peptide as shown above. Ongoing research efforts in our laboratory are directed at the incorporation of bioactive sequences into highly permeable cyclo(-D-Ala-Ala$_5$-) peptides to convey oral bioavailability. If the procedure presented here holds equally good for other systems, a long-standing problem in medicinal chemistry of peptides would be solved.

EXPERIMENTAL SECTION

Peptide synthesis and intestinal permeability are described in ref 26.

Reverse Phase HPLC. HPLC-ESI-MS analyses were performed on a Hewlett-Packard Series HP 1100 system with a Finnigan LCQ mass spectrometer using a YMC-Hydrosphere C18 column (12 nm pore size, 3 μm particle size, 125 mm × 2.1 mm). The system uses H_2O (0.1% formic acid) and MeCN (0.1% formic acid) as eluents. The same linear gradients (10−90% MeCN within 9 min at a flow rate of 0.55 mL/min) were applied for all peptides and testosterone at a temperature of 35 °C.

NMR Spectroscopy. 1D ^{1}H NMR, TOCSY, ROESY, and ^{13}C-HMBC spectra were recorded at 300 K on a Bruker Avance III spectrometer operating at 500 MHz. Samples were prepared in DMSO-d_6 at concentrations of 5−40 mM in 3 mm NMR tubes. DMSO-d_6 (^{1}H at 2.52 ppm, ^{13}C at 40.45 ppm) was used as internal standard. Data were processed with Topspin 1.3 software from Bruker. The homo- and heteronuclear experiments were recorded with spectral widths that were just sufficient to display all resonances in the respective dimensions (^{1}H: 8−10 ppm; ^{13}C: 190 ppm). The increments in t1 and t2 were adjusted to the information extracted from the individual experiments, ranging from 256 to 1024 increments in t1 and from 4096 to 8192 complex data points in t2. Depending on the individual experiments, 8 to 48 transients were averaged for each t1 value. A mixing time of 80 ms was used for TOCSY (spin-lock field, 6.25 kHz; mixing sequence MLEV17). The sequential assignments were obtained from heteronuclear J correlations that were extracted from HMBC spectra. Compensated ROESY experiments, which were used for the extraction of interproton distances, were performed with 100 ms mixing time and with spin-lock fields of 4 kHz.[36] The spin-lock was achieved using a train of 15° pulses. The volume integrals of the individually assigned cross-peaks were compensated for offset effects and converted into distance constraints using the isolated spin pair approximation.[37] In order to compensate for multiplicity of methyl groups, distances were multiplied by $(n_i n_j)^{1/6}$, where n_i and n_j are the numbers of the underlying degenerated protons i and j, respectively. After correction for multiplicity effects, 10% of the distances were added and subtracted in order to obtain upper and lower bounds. In order to compensate for bias that originates from using pseudoatoms, 0.4 Å were added on upper bounds of restraints involving one methyl group and 0.8 Å were added on upper bounds of restraints between two methyl groups. For calibration against intraresidual H^α−H^β distances, one-third of the average of the offset compensated intraresidual H^α−H^β crosspeak volumes was used as reference intensity. The average of the three distances between the α hydrogen atom and one of the three β hydrogen atoms in the sc+, sc-, and trans rotamers (=2.58 Å) was used as reference distance.

Distance Geometry Calculations. A home-written distance geometry program was used for metric matrix distance geometry calculations.[38] Beyond the geometric distance bounds (holonomic restraints), experimental distance restraints were placed in the final distance matrix whenever the latter were more restrictive. Upon random metrization, 50 template structures were embedded in four dimensions and partially minimized using conjugate gradient minimization. The following distance bound driven dynamics (DDD) simulation[39] was carried out in two subsequent steps (100 ps at 500 K, 40 ps at 1 K). Holonomic and experimental distance constraints plus a chiral penalty function were used in the DDD simulation to generate violation energies and forces. For each four-dimensional structure, a distance matrix was derived that served for the computation of coordinates in three dimensions using the EMBED algorithm. Another conjugate gradient minimization step, DDD simulations (100 ps at 500 K, 60 ps at 1 K), and two more conjugate gradient minimization steps were carried out to optimize the structures under the influence of distance constraints and chiral penalty functions. Distance restraints involving methyl groups were referred to pseudoatoms in the structure calculation process. The coordinates of the pseudoatoms were calculated as the arithmetic mean of the corresponding three methyl proton coordinates.

Molecular Dynamics Simulations. The GROMACS 4.0 software package (www.gromacs.org)[40−42] was used to perform energy minimizations and MD simulations in explicit DMSO. Visualization of the simulation trajectories was performed using the software packages VMD[43] and SYBYL.[44] The CHARMM27 force field,[45,46] was used for the molecular dynamics simulations. Periodic boundary conditions were employed on an octahedral simulation box, which was built with a distance of 3.1 nm for the solute, that consisted of ∼2000 DMSO molecules. Cut off distances of 1.4 nm for electrostatic and Lennard-Jones nonbonding interactions were applied. Simulation time steps were set to 2 fs. Constraints were imposed using the SHAKE method.[47] Temperature and pressure control was executed by Berendsen coupling.[48]

Equilibration of the system comprised an initial minimization of the DMSO solvent and subsequent 25 ps MD simulations at 50, 100, 150, 200, 250, and 300 K using position restraints. Subsequent temperature and pressure equilibrations were performed at every single temperature. Within the individual equilibration steps, the temperature was gradually increased, while the force constants of the position restraints were decreased exponentially from 250000 kJ mol^{-1} nm^{-2} at 50 to 25 kJ mol^{-1} nm^{-2} at 250 K. At 300 K no position restraints were applied and the temperature and pressure equilibrations were both extended to 50 ps. The final 2 ns MD simulations were carried out at 300 K.

ASSOCIATED CONTENT

Supporting Information

Assignments of ^{1}H and ^{13}C resonances, comparisons of chemical shifts of different peptides, distance restraints lists, temperature dependencies of the amide proton resonances, and some complementary results. This material is available free of charge via the Internet at http://pubs.acs.org.

AUTHOR INFORMATION

Corresponding Author

kessler@tum.de

Notes

The authors declare no competing financial interest.

ACKNOWLEDGMENTS

These studies were supported by the excellence initiative CIPSM and by SFB 594 of the Deutsche Forschungsgemeinschaft. J.G.B. thanks the TUM graduate school for support.

REFERENCES

(1) Lipinski, C. A.; Lombardo, F.; Dominy, B. W.; Feeney, P. J. *Adv. Drug Delivery Rev.* **2001**, *46*, 3−26.

(2) Veber, D. F.; Johnson, S. R.; Cheng, H. Y.; Smith, B. R.; Ward, K. W.; Kopple, K. D. *J. Med. Chem.* **2002**, *45*, 2615−2623.

(3) Zhang, M. Q.; Wilkinson, B. *Curr. Opin. Biotechnol.* **2007**, *18*, 478−488.

(4) Wieland, T.; Faulstich, H. *CRC Crit. Rev. Biochem.* **1978**, *5*, 185−260.
(5) Tjia, J. F.; Webber, I. R.; Back, D. J. *Br. J. Clin. Pharmacol.* **1991**, *31*, 344−346.
(6) Kolars, J. C.; Awni, W. M.; Merion, R. M.; Watkins, P. B. *Lancet* **1991**, *338*, 1488−1490.
(7) Bauer, W.; Briner, U.; Doepfner, W.; Haller, R.; Huguenin, R.; Marbach, P.; Petcher, T. J.; Pless, J. *Life Sci.* **1982**, *31*, 1133−1140.
(8) Cathapermal, S. S.; Foegh, M. L.; Rau, C. S.; Ramwell, P. W. *Drug Metab. Dispos.* **1991**, *19*, 735−739.
(9) Biron, E.; Chatterjee, J.; Ovadia, O.; Langenegger, D.; Brueggen, J.; Hoyer, D.; Schmid, H. A.; Jelinek, R.; Gilon, C.; Hoffman, A.; Kessler, H. *Angew. Chem., Int. Ed.* **2008**, *47*, 2595−2599.
(10) Dahlem, A. M.; Hassan, A. S.; Swanson, S. P.; Carmichael, W. W.; Beasley, V. R. *Pharmacol. Toxicol.* **1989**, *64*, 177−181.
(11) Hess, S.; Linde, Y.; Ovadia, O.; Safrai, E.; Shalev, D. E.; Swed, A.; Halbfinger, E.; Lapidot, T.; Winkler, I.; Gabinet, Y.; Faier, A.; Yarden, D.; Xiang, Z.; Portitlo, F. P.; Haskell-Luevano, C.; Gilon, C.; Hoffman, A. *J. Med. Chem.* **2008**, *51*, 1026−1034.
(12) Fjellestad-Paulsen, A.; Höglund, P.; Lundin, S.; Paulsen, O. *Clin. Endocrinol.* **1993**, *38*, 177−182.
(13) Lundin, S.; Vilhardt, H. *Acta Endocrinol. (Copenh.)* **1986**, *112*, 457−460.
(14) Sivonen, K.; Kononen, K.; Carmichael, W. W.; Dahlem, A. M.; Rinehart, K. L.; Kiviranta, J.; Niemela, S. I. *Appl. Environ. Microbiol.* **1989**, *55*, 1990−1995.
(15) Francis, G. *Nature* **1878**, *18*, 11−12.
(16) Edler, L.; Ferno, S.; Lind, M. G.; Lundberg, R.; Nilsson, P. O. *Ophelia* **1985**, *24*, 103−109.
(17) Gussmann, H.; Molzahn, M. J.; Bicks, B. *Monatsh. Veterinaermed.* **1985**, *40*, 76−79.
(18) White, T. R.; Renzelman, C. M.; Rand, A. C.; Rezai, T.; McEwen, C. M.; Gelev, V. M.; Turner, R. A.; Linington, R. G.; Leung, S. S. F.; Kalgutkar, A. S.; Bauman, J. N.; Zhang, Y. Z.; Liras, S.; Price, D. A.; Mathiowetz, A. M.; Jacobson, M. P.; Lokey, R. S. *Nat. Chem. Biol.* **2011**, *7*, 810−817.
(19) Rezai, T.; Bock, J. E.; Zhou, M. V.; Kalyanaraman, C.; Lokey, R. S.; Jacobson, M. P. *J. Am. Chem. Soc.* **2006**, *128*, 14073−14080.
(20) Rezai, T.; Yu, B.; Millhauser, G. L.; Jacobson, M. P.; Lokey, R. S. *J. Am. Chem. Soc.* **2006**, *128*, 2510−2511.
(21) Pauletti, G. M.; Okumu, F. W.; Borchardt, R. T. *Pharm. Res.* **1997**, *14*, 164−168.
(22) Knipp, G. T.; Velde, D. G. V.; Siahaan, T. J.; Borchardt, R. T. *Pharm. Res.* **1997**, *14*, 1332−1340.
(23) Kim, D. C.; Burton, P. S.; Borchardt, R. T. *Pharm. Res.* **1993**, *10*, 1710−1714.
(24) Gray, R. A.; Vandervelde, D. G.; Burke, C. J.; Manning, M. C.; Middaugh, C. R.; Borchardt, R. T. *Biochemistry* **1994**, *33*, 1323−1331.
(25) Fricker, G.; Drewe, J. *J. Pept. Sci.* **1996**, *2*, 195−211.
(26) Wieland, T.; Nassal, M.; Kramer, W.; Fricker, G.; Bickel, U.; Kurz, G. *Proc. Natl. Acad. Sci. U. S. A.* **1984**, *81*, 5232−5236.
(27) Ziegler, K.; Frimmer, M.; Kessler, K.; Damm, I.; Eiermann, V.; Koll, S.; Zarbock, J. *Biochim. Biophys. Acta* **1985**, *845*, 86−93.
(28) Ovadia, O.; Greenberg, S.; Chatterjee, J.; Laufer, B.; Opperer, F.; Kessler, H.; Gilon, C.; Hoffman, A. *Mol. Pharmaceutics* **2011**, *8*, 479−487.
(29) Kessler, H.; Matter, H.; Gemmecker, G.; Kling, A.; Kottenhahn, M. *J. Am. Chem. Soc.* **1991**, *113*, 7550−7563.
(30) Venkatachalam, C. M. *Biopolymers* **1968**, *6*, 1425−1436.
(31) Loosli, H.-R.; Kessler, H.; Oschkinat, H.; Weber, H.-P.; Petcher, T. J.; Widmer, A. *Helv. Chim. Acta* **1985**, *68*, 682−704.
(32) Klages, J.; Neubauer, C.; Coles, M.; Kessler, H.; Luy, B. *ChemBioChem* **2005**, *6*, 1672−1678.
(33) Laufer, B.; Chatterjee, J.; Frank, A. O.; Kessler, H. *J. Pept. Sci.* **2009**, *15*, 141−146.
(34) Chatterjee, J.; Laufer, B.; Beck, J. G.; Helyes, Z.; Pinter, E.; Szolcsanyi, J.; Horvath, A.; Mandl, J.; Reubi, J. C.; Keri, G.; Kessler, H. *ACS Med. Chem. Lett.* **2011**, *2*, 509−514.
(35) Fricker, G.; Drewe, J.; Huwyler, J.; Gutmann, H.; Beglinger, C. *Br. J. Pharmacol.* **1996**, *118*, 1841−1847.
(36) Griesinger, C.; Ernst, R. R. *J. Magn. Reson.* **1987**, *75*, 261−271.
(37) Kumar, A.; Wagner, G.; Ernst, R. R.; Wüthrich, K. *J. Am. Chem. Soc.* **1981**, *103*, 3654−3658.
(38) Havel, T. F. *Prog. Biophys. Mol. Biol.* **1991**, *56*, 43−78.
(39) Mierke, D. F.; Geyer, A.; Kessler, H. *Int. J. Pept. Protein Res.* **1994**, *44*, 325−331.
(40) Lindahl, E.; Hess, B.; van der Spoel, D. *J. Mol. Model.* **2001**, *7*, 306−317.
(41) van der Spoel, D.; Lindahl, E.; Hess, B.; Groenhof, G.; Mark, A. E.; Berendsen, H. J. C. *J. Comput. Chem.* **2005**, *26*, 1701−1718.
(42) van der Spoel D., Lindahl E., Hess B., van Buuren A. R., Apol P. J., Meulenhoff P. J., Tieleman D. P., Sijbers A. L. T. M., Feenstra K. A., van Drunen R., Berendsen H. J. C. *GROMACS User Manual*, version 4.0; 2005.
(43) Humphrey, W.; Dalke, A.; Schulten, K. *J. Mol. Graph.* **1996**, *14* (33−38), 27−38.
(44) SYBYL 8.0; Tripos International: 1699 South Hanley Rd., St. Louis, MI, 63144, USA.
(45) MacKerell, A. D.; Banavali, N.; Foloppe, N. *Biopolymers* **2000**, *56*, 257−265.
(46) Brooks, B. R.; Bruccoleri, R. E.; Olafson, B. D.; States, D. J.; Swaminathan, S.; Karplus, M. *J. Comput. Chem.* **1983**, *4*, 187−217.
(47) Ryckaert, J. P.; Ciccotti, G.; Berendsen, H. J. C. *J. Comput. Phys.* **1977**, *23*, 327−341.
(48) Berendsen, H. J. C.; Postma, J. P. M.; van Gunsteren, W. F.; Dinola, A.; Haak, J. R. *J. Chem. Phys.* **1984**, *81*, 3684−3690.